



Lithospheric structure of Taiwan from gravity modelling and sequential inversion of seismological and gravity data

F. Masson ^{a,*}, M. Mouyen ^{a,b}, C. Hwang ^b, Y.-M. Wu ^c, F. Ponton ^a, M. Lehujeur ^a, C. Dorbath ^a

^a IPGS CNRS/University Strasbourg, Strasbourg, France

^b National Chiao Tung University, Hsinchu, Taiwan

^c National Taiwan University, Taipei, Taiwan

ARTICLE INFO

Article history:

Received 11 July 2011

Received in revised form 21 February 2012

Accepted 11 April 2012

Available online 24 April 2012

Keywords:

Seismic tomography

Gravity

Taiwan

Simultaneous inversion

ABSTRACT

Using a Bouguer anomaly map and a dense seismic data set, we have performed two studies in order to improve our knowledge of the deep structure of Taiwan.

First, we model the Bouguer anomaly along a profile crossing the island using simple forward modelling. The modelling is 2D, with the hypothesis of cylindrical symmetry.

Second we present a joint analysis of gravity anomaly and seismic arrival time data recorded in Taiwan. An initial velocity model has been obtained by local earthquake tomography (LET) of the seismological data. The LET velocity model was used to construct an initial 3D gravity model, using a linear velocity–density relationship (Birch's law). The synthetic Bouguer anomaly calculated for this model has the same shape and wavelength as the observed anomaly. However some characteristics of the anomaly map are not retrieved. To derive a crustal velocity/density model which accounts for both types of observations, we performed a sequential inversion of seismological and gravity data. The variance reduction of the arrival time data for the final sequential model was comparable to the variance reduction obtained by simple LET. Moreover, the sequential model explained about 80% of the observed gravity anomaly. New 3D model of Taiwan lithosphere is presented.

© 2012 Elsevier B.V. All rights reserved.

1. Introduction

The island of Taiwan is at the junction of the Philippine Sea plate and the Eurasian plate (Fig. 1) and results from the convergence of the Luzon volcanic arc on the Philippine Sea plate toward the Chinese continental margin on the Eurasian plate. In the northeast, the Philippine Sea plate subducts below the Eurasian plate along the Ryukyu Trench. In the south, the situation is reversed and the Eurasian plate subducts below the Philippine Sea plate along the Manila Trench (Angelier, 1986). In Taiwan, the Longitudinal Valley separating the Eurasian plate to the west and the Philippine Sea plate to the east underlines the plate boundary. No tectonic style of the collision between the Luzon arc and the Chinese continental margin is unanimously accepted. Two main hypotheses are generally discussed: thin-skinned tectonics (Dahlen et al., 1984; Davis et al., 1983; Suppe, 1980) and thick-skinned tectonics (Hung et al., 1999; Mouthereau and Petit, 2003; Wu et al., 1997).

1.1. Thin-skinned tectonics

This hypothesis assumes that the orogenic wedge of Taiwan grows by frontal accretion of the Chinese continental margin materials above

a shallow detachment (~10 km), gently dipping eastward. The wedge is deformed by the convergence of the Philippine Sea plate until a critical state that makes it break, eventually shaping a fold-and-thrusts belt (Chapple, 1978). Davis et al. (1983) develop an analytic theory that predicts the critical deformation of the prism materials in a compressive context. They quantitatively test this theory for the Taiwanese accretionary prism and obtain results in agreement with field observations. They suggest that the detachment is at the basal part of the Neogene continental margin. Dahlen et al. (1984) identified it more precisely in the Miocene and Pliocene layers. To define the thin-skinned cross section (Fig. 3a), we use a model inspired from the cross-section drawn by Malavieille and Trullenque (2009).

1.2. Thick-skinned tectonics

Some authors, using seismological data from the Taiwan front orogen (Wu et al., 1997) or well-log and seismic reflection data (Hung et al., 1999) disagree with the thin-skinned tectonic model. According to Wu et al. (1997), the Taiwanese orogeny involves the whole crust and the upper mantle, in particular beneath the Central Range. They suggest lithospheric collision between the Eurasian and the Philippine Sea plates. The thick-skinned tectonic model (Fig. 3b) was constructed from the models proposed by Yamato et al. (2009) and Yen et al. (1998).

* Corresponding author. Tel.: +33 3 68 85 50 29.

E-mail address: frederic.masson@unistra.fr (F. Masson).

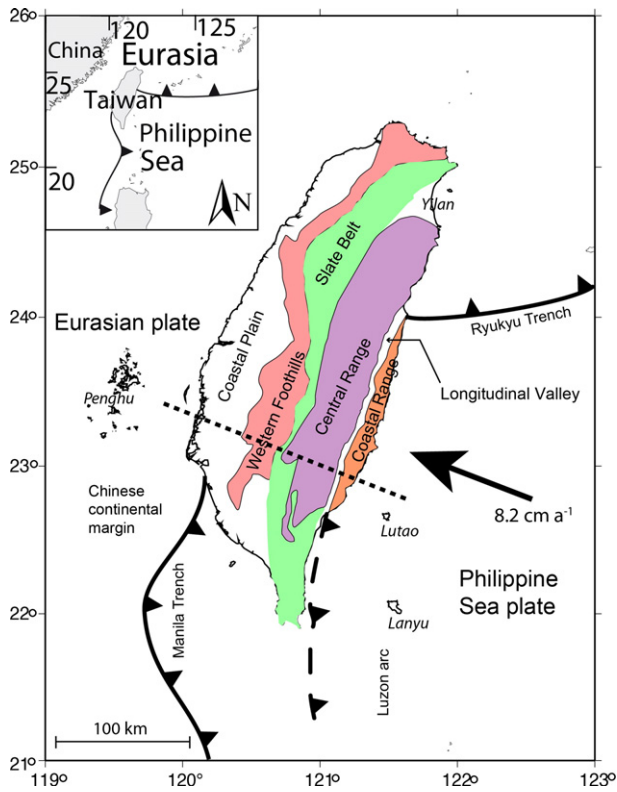


Fig. 1. Taiwan tectonic and geologic settings (after Hickman et al., 2002; Ho, 1986; Mouyen et al., 2009). The dashed line indicates the cross-section shown in Fig. 8. Numbers 1 to 6 are geological regions, 1: Coastal Plain; 2: Western Foothills; 3: Slate Belt; 4: Central Range; 5: Longitudinal Valley; 6: Coastal Range.

A good knowledge of the 3D structure of Taiwan is a very important foundation for a variety of earthquake research topics, such as earthquake relocation, earthquake source study and the understanding of the active structural characteristics and the tectonic evolution of the collision zone. To this end, there has been a long history of attempts in imaging the structure in the Taiwan region (Kim et al., 2005; Ma et al., 1996; Rau and Wu, 1995; Shin and Chen, 1998; Wu et al., 2007, 2009).

At crustal scale, the more usual approach is to perform a local earthquake tomography (LET), which allows the simultaneous determination of a 3D seismic velocity model and earthquake locations. Another approach is to perform gravity modelling, generally starting from 2D models and continuing toward 3D models. When gravity and seismic data are both available, it is beneficial to perform a simultaneous inversion to obtain seismic velocity and density models, as well as earthquake locations. This simultaneous inversion is justified by the fact that independent seismic models are generally not able to explain correctly the observed gravity anomaly while the simple density models are not uniquely constrained. This will be clearly shown for Taiwan in the next sections.

2. Gravity data and forward gravity modelling

2.1. Gravity data

Fig. 2 shows the compiled Bouguer anomaly map used in this study (Hwang et al., 2007). This map results from the downward continuation of an airborne Bouguer gravity map computed at 5 km high. This allows:

1– a homogeneous coverage of Taiwan, which is not realisable otherwise due to the low number of existing gravity measurements in the Central Range.

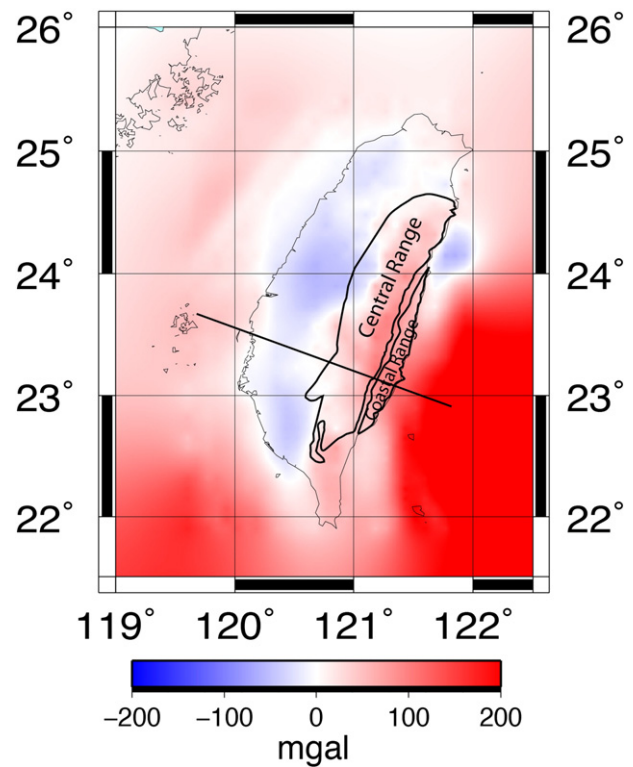


Fig. 2. Bouguer anomalies at sea level computed from downward continuation of airborne gravity anomalies at 5000 m (Hwang et al., 2007). The black line locates the cross-sections shown in Figs. 3 and 4. Contour lines of the Central and Coastal Ranges are from Fig. 1.

2– The computation of models at sea level because the topography has been corrected before the downward continuation.

The lateral extension of the Bouguer anomaly map offshore allows the computation of models extended far from the coastline of Taiwan.

At large scale the map reflects the large structures of Taiwan. The Bouguer anomaly is positive above the Coastal Range, the Longitudinal Valley and the eastern part of the Central Range. This indicates that this region is not in isostatic equilibrium, which should be characterised by a negative Bouguer anomaly, as it can be seen in the Alps (Masson et al., 1999). The highest values of the Bouguer anomaly are observed along the Coastal Range probably due to high-density volcanic rocks. Negative anomalies are observed in western Taiwan along the Slate Belt, the Western Foothills and the Coastal Plain. This is related to low density sedimentary rock (between 1.96 and 2.0 (Telford et al., 1990)). Marine Bouguer anomalies clearly allow distinguishing oceanic and continental crust. In the north and the west of Taiwan, slightly positive anomalies indicate continental crust. The southeast and southwest positive anomalies correspond to the Philippine Sea and Eurasian oceanic crust respectively. The northeast positive anomaly corresponds to the sedimentary accretionary basin resulting from the subduction of the Philippine Sea plate below the Eurasian Plate along the Ryukyu Through.

In the Fig. 3a and b we present the gravity effects of density models computed using the Talwani et al. (1959) method along the profile drawn in Fig. 2.

2.2. Forward modelling

The cross-section is made between latitudes 23°N and 23.5°N, and is perpendicular to the collision front. At these latitudes, the collision is older and therefore more mature. The thin- and thick-skinned

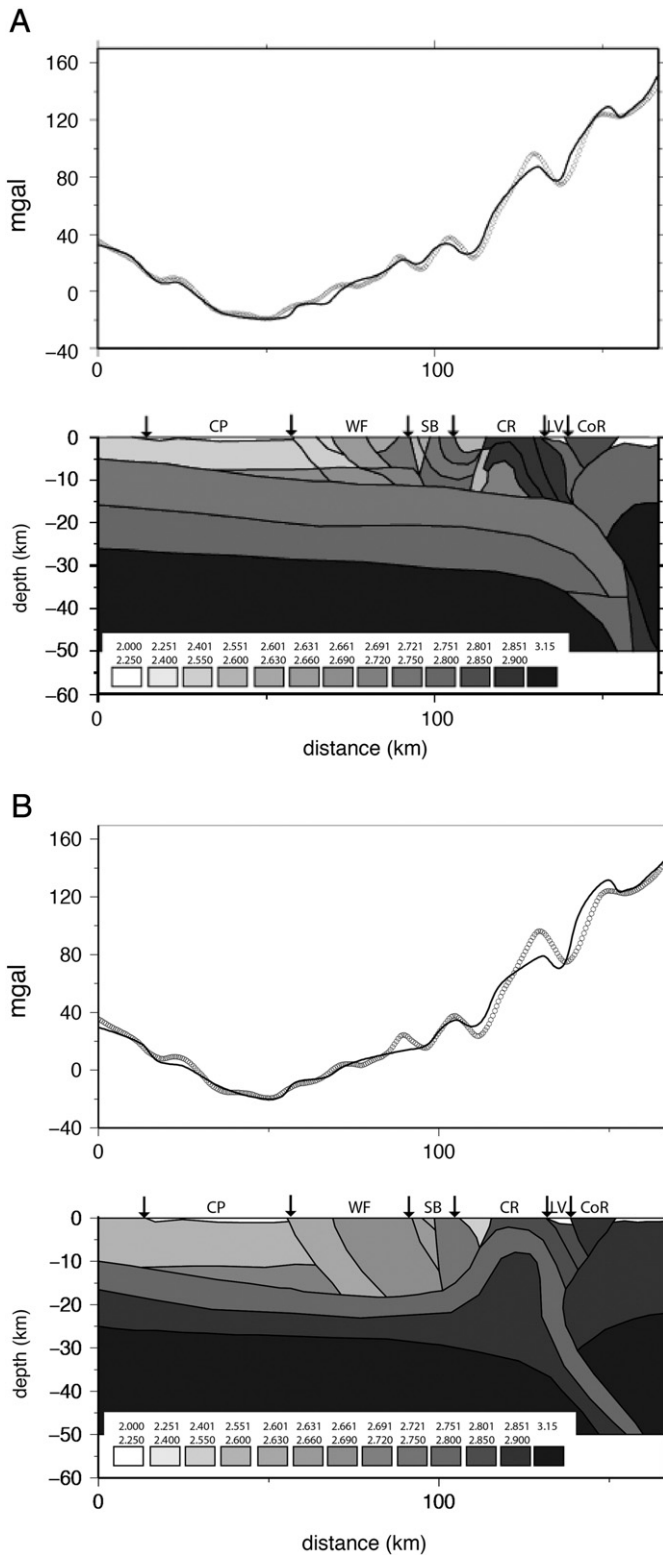


Fig. 3. (a) Gravity modelling (see location in Fig. 2). Top: Observed (black) and modelled (grey) gravity anomaly. Bottom: Density model obtained from thin-skinned hypothesis (see text for details). CP: Coastal Plain, WF: Western Foothills, SB: Slate Belt, CR: Central Range, LV: Longitudinal Valley, CoR: Coastal Range. (b) Same as (a) for the thick-skinned hypothesis.

tectonic schemes will be discussed below. The geometry of the island cross-section will be different depending on the hypothesis taken into account and, consequently, the results of the modelling too. In this study, both will be used to see their effects in terms of gravity.

Thin-skinned (Fig. 3a) and thick-skinned (Fig. 3b) models have been built by trying to best comply with the following constraints:

- At the surface, the limits of the structures are identical in both models, consistent with surface geology.
- In agreement with the seismological data published by Wu et al. (1997), Moho depth was fixed at 28 km beneath the Western Foothills, 38 km beneath the Central Range and 20 km beneath the Coastal Range.
- The decollement was made at 10 km and 15 km depth for the thin-skinned and thick-skinned models, respectively.

In a first step, only the shape of the structures has been changed from one model to another. In a second step, densities have been slightly adjusted. For the pre-Tertiary basement of the Chinese continental margin, the densities that best fit both models simultaneously are 2.76 g/cm³ for the upper and 2.82 g/cm³ for the lower crust. Density of the Coastal Plain and the Longitudinal Valley is about 2.1 g/cm³, consistent for sedimentary layers. The densities proposed for the accretionary prism overlying the Chinese continental margin were chosen between 2.6 g/cm³ and 2.8 g/cm³ depending on the nature of the rocks (mainly sandstone, shale, clay and slate) and the degree of metamorphism which increases approaching the Longitudinal Valley (Ho, 1986).

Although the thin-skinned model allows a better fit of the data than the thick-skinned model (RMS of 4.0 mgal and 6.46 mgal respectively), both models are likely to explain the overall shape of the observed anomaly. This confirms the well-know fact that gravity data alone are not able to univocally constrain the structural model. Next we propose the simultaneous inversion of gravity and seismological data.

3. Simultaneous inversion of the gravity and seismological data

Another way to use the gravity data is to perform inverse modelling jointly with seismological inversion (Kaufmann and Long, 1996; Lees and VanDecar, 1991; Lines et al., 1988; Oppenheimer and Herkenhoff, 1981; Tiberi et al., 2003; Tiberi et al., 2008; Vernant et al., 2002). This approach is interesting for two main reasons:

- 1- Seismic velocities can be converted to density. Therefore, the use of seismological data allows constraining the density model, which is generally not uniquely constrained by forward gravity modelling, as it has been shown in Sections 2–3.
- 2- Conversely the seismological models are generally not able to fully explain the gravity data and can be refined by gravity data. Moreover, the gravity data are much more evenly distributed than the seismological one, and thus offer a continuous sampling of the region, which is not the case for the local seismicity.

Combining both data sets improves final seismic and gravity models. In a first step we will show that even in Taiwan, exceptional seismological data poorly fit the gravity data. To show this we perform a simple local earthquake tomography of Taiwan. Second, following the method of Vernant et al. (2002) we develop a joint seismic and gravity model.

3.1. Local earthquake tomography

In this study we strictly repeat the study of Wu et al. (2007) using the same seismological data set and the same LET method. We inverted arrival times simultaneously for velocity (V_p and V_p/V_s) and hypocenter parameters using the classical software SIMULPS (Eberhart-Philips, 1993; Evans et al., 1994; Thurber, 1983). A total of 299,104 P-wave arrival times and 174,203 S–P times were obtained from 17,206 regional earthquakes. The velocity model is specified on a set of 3D spatial gridpoints, and a linear interpolation is adopted between the gridpoints. A total of 19 gridpoints are distributed at the depths of 0, 2, 4, 6, 9, 13, 17, 21, 25, 30, 35, 50, 70, 90, 110, 140, 170, 200 and 400 km. In order to align the gridpoints to the main geological structures of Taiwan, the

grid is rotated 20° East. The horizontal grid spacings in west-northwest-east-southeast and north-northeast-south-southwest directions are 7.5 and 12.5 km, respectively, in the interior part of the grid, whereas the grid spacing for the offshore regions is 20 km. The difference in grid spacing is due to the difference in the path coverage, as well as the dominance of northeast-southwest trending geological features on the Island of Taiwan. Ray tracing is accomplished using an approximate 3-D algorithm with curved nonplanar ray paths (Um and Thurber, 1987), and the damped least-squares inversion is based on the parameter separation technique of Pavlis and Booker (1980). The damping values of 35 for Vp and 40 for Vp/Vs and the initial tabular velocity model are taken from Wu et al. (2007).

The model obtained from the inversion is identical to the one obtained by Wu et al. (2007) and will be described in Section 4.

3.2. Failure of the direct modelling of gravity data from the initial LET model

In the forward approach, the Vp model is converted into an a priori density model to calculate the gravity effect of crustal heterogeneities. The empirical Birch (1961) is commonly used to define the linear relationship between density and P wave velocity. In order to calculate the theoretical gravity field, the crust is partitioned in prismatic elementary cells with uniform density. To do this, we adopt the space discretisation of the LET model of Wu et al. (2007) described above.

At a first glance, the resulting map (Fig. 4) looks similar to the observed gravity map. The east-west contrast from the Coastal Plain to the Coastal Range and the well-defined boundaries of the Philippines Sea Plate are clearly observed on both maps. However, several differences can be identified: the spatial extension and the amplitude of the negative anomaly of the main island are not consistent; the oceanic crust of the Chinese continental margin which is underlined by a positive gravity anomaly is not retrieved; conversely, a positive anomaly below the Penghu Islands (China Sea) shown from the seismological model is not observed in the gravity data; the negative anomaly related to the accretionary prism of the Ryukyu trench is not retrieved, etc. Most of these differences are due to the lack of seismological data in these regions (no earthquake and/or no station) inducing a low resolution. The standard deviation for the gravity field is 45 mgal.

Yen and Hsieh (2010) also observe this discrepancy between the gravity data and the gravity anomaly obtained from seismic models. Using three seismic velocity models obtained by Rau and Wu (1995), Kim et al. (2005) and Wu et al. (2007) and the conversion

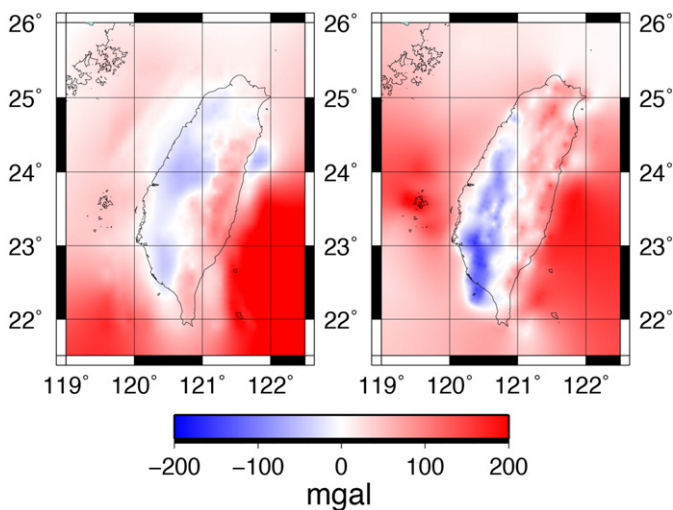


Fig. 4. Left: Bouguer anomaly map of Fig. 2. Right: Synthetic Bouguer anomaly map computed from the local earthquake tomography model converted to density using Birch (1961).

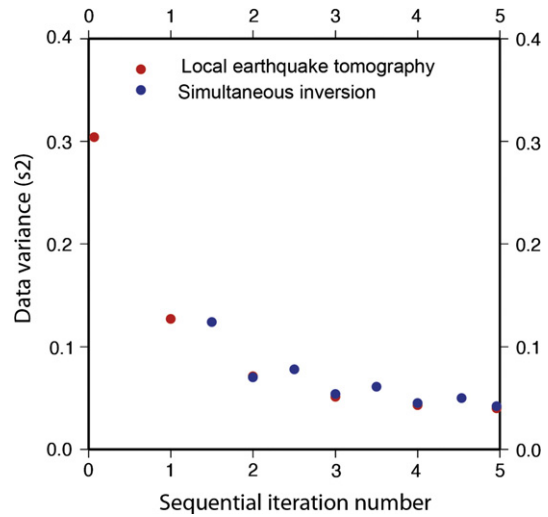


Fig. 5. Red dots: Variance of the seismic data versus the number of iteration for the LET performed following Wu et al. (2007). Blue dots: Variance of the seismic data versus the number of iteration for the sequential inversion. The blue dots collocated with the red ones give the variance after the seismic inversions. The other blue dots give the variance after the gravimetric inversions. These inversions decrease the variance only for the first iteration. Red and blue dots show similar variance reduction indicating that the cooperative inversion explains the seismic data as well as the simple seismic inversion.

law of Ludwig et al. (1970) and Barton (1986), they are not able to get a perfect fit between observed and computed anomalies.

In order to obtain a velocity model that explains the gravity data, we decided to use a cooperative inversion (Lines et al., 1988) of the two data sets in order to compute a 3D velocity-density model consistent with both gravity and seismic data.

3.3. Sequential inversion of the seismological and gravity data

Lines et al. (1988) propose two main kinds of cooperative inversion of geophysical data. The first one is the joint inversion where all data are inverted simultaneously. This strategy is often used for data sets combining gravity and seismics (Kaufmann and Long, 1996; Lees and VanDecar,

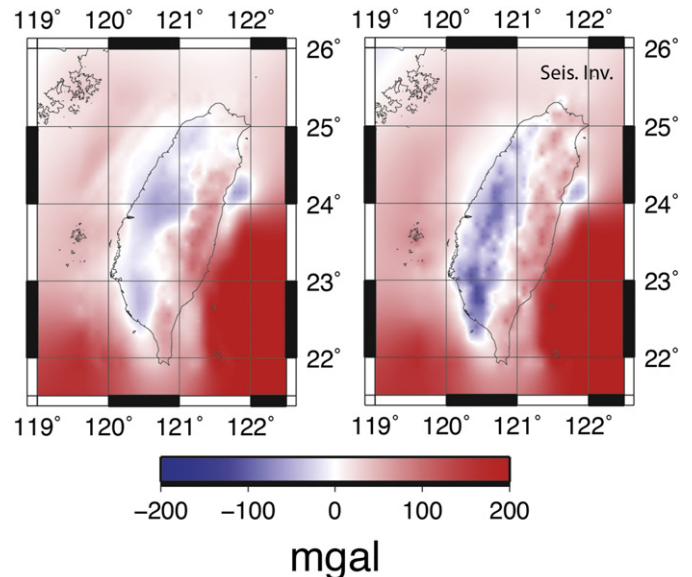


Fig. 6. Left: Bouguer anomaly map of Fig. 2. Right: Synthetic Bouguer anomaly computed from the final sequential model.

1991; Oppenheimer and Herkenhoff, 1981; Tiberi et al., 2003; Tiberi et al., 2008). The second one is the sequential inversion where each data set is successively inverted. The a posteriori information resulting from the previous inversion of the first data set is transformed into a priori information to invert the second data set. To re-use the SIMULPS inversion method previously applied by Wu et al. (2007) for the LET, we adopt the sequential strategy. We strictly follow the approach presented by Vernant et al. (2002), which consists of the reiteration of one inversion of the seismological inversion, leading to new velocity model and new event locations, followed by one inversion of the gravity data and the computation of a new density model. Using this method, it is possible to qualitatively estimate what information is brought to the model by seismic and gravity data. The starting velocity model used for the first inversion of travel time data is the initial 1D velocity model estimated by Wu et al. (2007). Then, the iterative SIMULPS software calculates the 3D Vp model and new earthquake locations from the arrival times of local earthquakes. This process is stopped after one iteration. This 3D absolute Vp model is then converted into a 3D density model using the Birch's law. At this stage, the linear inverse gravity problem is solved leading to a new density model that is transformed back to a new Vp model. This completes the first loop of the sequential inversion. The following loops use the same procedure defining as input the

final velocity model of the previous loop. The sequential process is stopped when the standard deviations between observed data and theoretical values calculated from the models stop decreasing significantly between two loops.

The curves showing variance reductions on travel time data are shown in Fig. 5. The standard deviations do not change significantly after the fourth iteration. We stop the process after 5 iterations. The variance of the time delays decreases from 0.303 s^2 to 0.041 s^2 . The standard deviation for the gravity field reduces from 60 mgal to 10 mgal. Note that although Wu et al. (2007)'s final model variance (0.038 s^2) after 5 iterations is slightly smaller than the one we obtain here (0.041 s^2), their model poorly fits the gravity data (35 mgal versus 10 mgal). However, the difference is small and our model explains gravity data. A careful look at Fig. 5 shows that the variance decreases after the first gravimetric inversion, implying that the gravity data significantly improves the velocity model. After a few iterations the gravity inversion slightly degrades the velocity model.

Fig. 6 shows the final gravity model. The main differences observed in Fig. 4 are corrected. Even if the amplitude remains too high, the form of the main negative anomaly is well retrieved, both in its east–west extension and in its Northward extension. The other differences (oceanic crust of the China Sea, Penghu Island anomaly, Ruykyu sedimentary

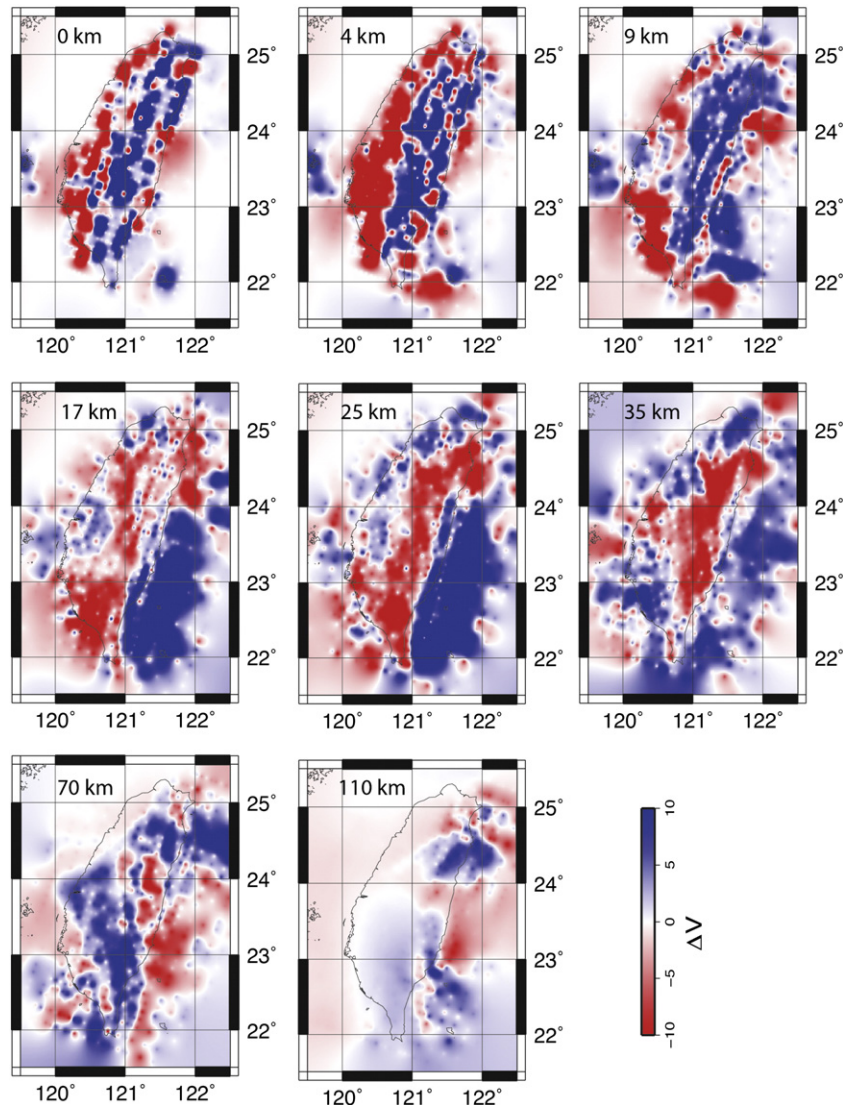


Fig. 7. P-wave velocity maps obtained by sequential inversion. In shallow (<10 km deep) layers, Vp anomalies are associated with near-surface geologic units and high Vp coincides with the high mountain ranges. At greater depth (17 and 25 km depth), strong West (low)–East (high) velocity contrast is observed located along the Longitudinal Valley. Further below, the low velocity zone appears to gradually sink eastward.

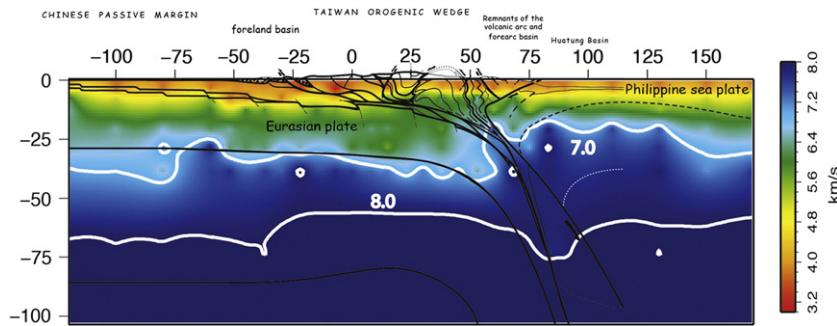


Fig. 8. Vertical cross-sections through the sequential model along the line drawn in Fig. 1. Geological model drawn by Malavieille and Trullenque (2009) along the same profile has been superimposed (black lines). The cross-section emphasises the structures observed in Fig. 7.

basins) are corrected. With our sequential approach, we find a 3-D velocity model that explains the traveltimes and the gravity data.

4. Discussion

The 3D Vp structure from our inversion largely agrees with that obtained in Wu et al. (2007) (Fig. 7). In shallow (<10 km deep) layers, Vp anomalies are associated with near-surface geologic units. Low Vp structures are mainly associated to young sediments of the coastal basins and the Western Foothills. In the first layer (0 km depth) smaller low velocity areas near Yilan and the ends of the Longitudinal Valley may also correspond to large amount of sediments. Farther east, high Vp coincides with the high mountain ranges of Taiwan, including the Slate Belt and the Central Range. Highest velocities underline the volcanic rocks of the Coastal Range. At greater depth (17 and 25 km depth), low velocities are covering a large part of the island, from the Western Foothills to the Central Range. A sharp north-south boundary limits the low velocity zone to the East. High velocities are related to the Longitudinal Valley and the Coastal Range. At greater depth the low velocity zone appears to gradually sink eastward.

The cross-section emphasises features observed on the map (Fig. 8). At shallow depth, low velocities (red–yellow) are located from –50 to 0 km, which corresponds to the Western Foothills and the foreland basin. This low velocity layer thins westward from the Slate Belt to the Coastal Range. At greater depth a sharp contrast is observed at the Longitudinal Valley. West of the Longitudinal Valley, the upper crust (velocity lower than 7.0 km/s) thickens westward. East of the Longitudinal Valley high velocities are observed at shallow depth. The vertical step of the 7.0 km/s contour line is of about 15 km. This is roughly consistent with the Moho depth step observed using teleseismic receiver functions from the Central Range to the Coastal Range (Wang et al., 2010). At great depth, as shown by the 8 km/s contour line, low velocity material from the Eurasian lithosphere seems to be underthrusting the Philippine Sea Plate lithosphere. The sequential inversion of gravity and seismological data provides a model that appears to be in close agreement with the model drawn by Malavieille and Trullenque (2009) based on geological data and analogue modelling (Fig. 8). All the features proposed in this model are obtained in the velocity model: sedimentary basins (–50 to 0 km), thickening of the crust (0 to 50 km), high velocity below the Central Range (25 to 50 km), sharp contrast at the longitudinal valley (~55 km), buried Eurasian lithosphere (75 to 100 km).

5. Conclusion

Many models of Taiwan obtained from seismic tomography have been proposed in recent years (Kim et al., 2005; Ma et al., 1996; Rau and Wu, 1995; Shin and Chen, 1998; Wu et al., 2007, 2009). These models describe with increasing accuracy the structure of Taiwan. In this study we look at the contribution of the gravity data to the improvement of our knowledge of deep structures. Computation of a theoretical gravity

anomaly from the local earthquake tomography model of Wu et al. (2007) points out that this model poorly explains the observed gravity field.

Two approaches have been tested: the forward modelling of gravity anomalies and the sequential inversion of gravity and seismological data. The forward modelling shows that it is possible to define density models that fit the observed gravity data. However, it is well known that a forward modelling of gravity anomalies leads to non-unique solutions. This has been shown from gravity modelling of a cross-section through the Taiwan Island. Both thin-skinned and thick-skinned models are able to explain the data. The gravity data is further inverted jointly with seismic data using a sequential approach, and the final models satisfy the two data sets. Generally, inversion of the gravity field completes the seismic tomography where rays are sparse. Finally we propose a structural model of the different structures of Taiwan and specially the contrast from the Eurasian and Philippines Sea plates, and enlightens the subduction.

References

- Angelier, J., 1986. Preface. *Tectonophysics* 125.
- Barton, P.J., 1986. The relationship between seismic velocity and density in the continental crust – a useful constraint? *Geophysical Journal of the Royal Astronomical Society* 87, 195–208.
- Birch, F., 1961. The velocity of compressional waves in rocks to 10 kilobars, part 2. *Journal of Geophysical Research* 66, 2199–2224.
- Chapple, W.M., 1978. Mechanics of thin-skinned fold-and-thrust belts. *Geological Society of America Bulletin* 89, 1189–1198.
- Dahlen, F.A., Suppe, J., Davis, D., 1984. Mechanics of fold-and-thrust belts and accretionary wedges: cohesive Coulomb theory. *Journal of Geophysical Research* 89 (B12), 10,087–10,101.
- Davis, D., Suppe, J., Dahlen, F.A., 1983. Mechanics of fold-and-thrust belts and accretionary wedges. *Journal of Geophysical Research* 88 (B2), 1153–1172.
- Eberhart-Philips, D., 1993. Local earthquake tomography: earthquake source regions. In: Iyer, H.M., Hirahara, K. (Eds.), *Seismic Tomography: Theory and Practice*. Chapman and Hall, London, pp. 613–643.
- Evans, J.R., Eberhart-Philips, D., Thurber, C.H., 1994. User's manual for SIMULPS12 for imaging Vp and Vp/Vs: a derivative of the "Thurber" tomographic inversion SIMUL3 for local earthquakes and explosions. *U.S. Geological Survey Open File Report* 94–431.
- Hickman, J.B., Wiltchko, D.V., Hung, J.H., Fang, P., Bock, Y., 2002. Structure and evolution of the active fold-and-thrust belt of southwestern Taiwan from Global Positioning System analysis. *Geological Society of America Special Papers* 358, 75–92.
- Ho, C.S., 1986. A synthesis of the geologic evolution of Taiwan. *Tectonophysics* 125, 1–16.
- Hung, J.-H., Wiltchko, D.V., Lin, H.-C., Hickman, J.B., Fang, P., Bock, Y., 1999. Structure and motion of the southwestern Taiwan fold-and-thrust belt. *TAO* 10 (3), 543–568.
- Hwang, C., Hsiao, Y., Shih, H., Yang, M., Chen, K., Forsberg, R., Olesen, A., 2007. Geodetic and geophysical results from a Taiwan airborne gravity survey: data reduction and accuracy assessment. *Journal of Geophysical Research* 112, B04407.
- Kaufmann, R.D., Long, L.T., 1996. Velocity structure and seismicity of southeastern Tennessee. *Journal of Geophysical Research* 101, 8531–8542.
- Kim, K.H., Chiu, J.M., Pujol, J., Chen, K.C., Huang, B.S., Yeh, Y.H., Shen, P., 2005. Three-dimensional Vp and Vs structural model associated with the active subduction and collision tectonics in the Taiwan region. *Geophysical Journal International* 162, 204–220.
- Lees, J.M., VanDecar, J.C., 1991. Seismic tomography constrained by Bouguer gravity anomalies: applications in western Washington. *Pure and Applied Geophysics* 135, 31–52.

- Lines, L.R., Schultz, A.K., Treitel, S., 1988. Cooperative inversion of geophysical data. *Geophysics* 53, 8–20.
- Ludwig, J.W., Nafe, J.E., Drake, C.L., 1970. In: Maxwell, A.E. (Ed.), *Seismic refraction. : The Sea*, 4. Wiley, New York, pp. 53–84.
- Ma, K.F., Wang, J.H., Zhao, D., 1996. Three-dimensional seismic velocity structure of the crust and uppermost mantle beneath Taiwan. *Journal of Physics Earth* 44, 85–105.
- Malavieille, J., Trullenque, G., 2009. Consequences of continental subduction on forearc basin and accretionary wedge deformation in SE Taiwan: insights from analogue modeling. *Tectonophysics* 466, 377–394.
- Masson, F., Verdun, J., Bayer, R., Debeglia, N., 1999. Une nouvelle carte gravimétrique des Alpes Occidentales et ses conséquences structurales et tectonique. *Comptes Rendus De L Academie Des Sciences Paris* 329, 865–871.
- Mouthereau, F., Petit, C., 2003. Rheology and strength of the Eurasian continental lithosphere in the foreland of the Taiwan collision belt: constraints from seismicity, flexure and structural styles. *Journal of Geophysical Research* 108 (B11), 2512, <http://dx.doi.org/10.1029/2002JB002098>.
- Mouyen, M., Masson, F., Hwang, C., Cheng, C., Cattin, R., Lee, C., Le Moigne, N., Hinderer, J., Malavieille, J., Bayer, R., Luck, B., 2009. Expected temporal absolute gravity change across the Taiwanese Orogen, a modeling approach. *Journal of Geodynamics* 48, 284–291.
- Oppenheimer, D.H., Herkenhoff, K.E., 1981. Velocity density properties of the lithosphere from three-dimensional modeling at the Geysers–Clear Lake Region, California. *Journal of Geophysical Research* 86, 6057–6065.
- Pavlis, G.L., Booker, J.R., 1980. The mixed discrete-continuous inverse problem: application to the simultaneous determination of earthquake hypocenters and velocity structure. *Journal of Geophysical Research* 85, 4801–4810.
- Rau, R.-J., Wu, F.T., 1995. Tomographic imaging of lithospheric structures under Taiwan. *Earth and Planetary Science Letters* 133, 517–532.
- Shin, T.C., Chen, Y.L., 1998. Study on the earthquake location of 3-D velocity structure in the Taiwan area. *Meteorological Bulletin* 42, 135–169.
- Suppe, J., 1980. A retrodeformable cross section of northern Taiwan. *Geological Society of China Proceedings* 23, 46–55.
- Talwani, M., Worzel, J.L., Landisman, M., 1959. Rapid gravity computations for two-dimensional bodies with application to the Mendocino submarine fracture zone. *Journal of Geophysical Research* 64, 49–59.
- Telford, W.M., Geldart, R.E., Sheriff, R.E., 1990. *Applied Geophysics*, 2nd ed. (Cambridge, UK).
- Thurber, C.H., 1983. Earthquake location and three-dimensional crustal structure in Coyote Lake area, Central California. *Journal of Geophysical Research* 88, 8226–8236.
- Tiberi, C., Diament, M., Deverchere, J., Petit-Mariani, C., Mikhailov, V., Tikhotsky, S., Achauer, U., 2003. Deep structure of the Baikal rift zone revealed by joint inversion of gravity and seismology. *Journal of Geophysical Research* 108 (B3), 2113, <http://dx.doi.org/10.1029/2002JB001880>.
- Tiberi, C., Deschamps, A., Deverchere, J., Petit, C., Perrot, J., Appriou, D., Mordvinova, V., Dugaarma, T., Ulzibaat, M., Artemiev, A.A., 2008. Asthenospheric imprints on the lithosphere in Central Mongolia and Southern Siberia from a joint inversion of gravity and seismology (MOBAL experiment). *Geophysical Journal International* 175 (3), 1283–1297.
- Um, J., Thurber, C.H., 1987. A fast algorithm for two-point seismic ray tracing. *Bulletin Seismological Society of America* 77, 972–986.
- Vernant, P., Masson, F., Bayer, R., Paul, A., 2002. Sequential inversion of local earthquake travel times and gravity anomaly – the example of the Western Alps. *Geophysical Journal International* 150, 79–90.
- Wang, H.-L., Zhu, L., Chen, H.-W., 2010. Moho depth variation in Taiwan from teleseismic receiver functions. *Journal of Asian Earth Sciences* 37, 286–291.
- Wu, F.-T., Rau, R.-J., Salzberg, D., 1997. Taiwan orogeny: thin-skinned or lithospheric collision? *Tectonophysics* 274, 191–220.
- Wu, Y.-M., Chang, C.-H., Zhao, L., Shyu, J.B.H., Chen, Y.-G., Sieh, K., Avouac, J.-P., 2007. Seismic tomography of Taiwan: improved constraints from a dense network of strong motion stations. *Journal of Geophysical Research* 112, B08312, <http://dx.doi.org/10.1029/2007JB004983>.
- Wu, Y.-M., Shyu, J.B.H., Chang, C.-H., Zha, L., Nakamura, M., Hsu, S.-K., 2009. Improved seismic tomography offshore northeastern Taiwan: implications for subduction and collision processes between Taiwan and the southernmost Ryukyu. *Geophysical Journal International* 178, 1042–1054.
- Yamato, P., Mouthereau, F., Burov, E., 2009. Taiwan mountain building: insights from 2-D thermomechanical modelling of a rheologically stratified lithosphere. *Geophysical Journal International* 176, 307–326.
- Yen, H.-Y., Hsieh, H.-H., 2010. A study on the compatibility of 3-D seismic velocity structures with gravity data of Taiwan. *Terrestrial Atmospheric and Oceanic Sciences* 21, 897–904.
- Yen, H.-Y., Yeh, Y.-H., Wu, F.T., 1998. Two-dimensional crustal structures of Taiwan from gravity data. *Tectonics* 17, 104–111.